DOI: 10.1002/cctc.201100223

# SBA-16-Supported Cobalt Catalyst with High Activity and Stability for Fischer–Tropsch Synthesis

Yanxi Zhao,[a, b] Yuhua Zhang,[a, b] Jian Chen,[b] Jinlin Li,*[b] Kongyong Liew,[b, c] and Mohd Ridzuan Bin Nordin[c]

SBA-16 molecular sieves were used as support to prepare cobalt catalyst for Fischer–Tropsch synthesis (FTS). The catalysts were characterized by using TEM, power XRD, temperature-programmed reduction, and $N_2$ adsorption–desorption. The analyses indicate that most of the $Co_3O_4$ nanoparticles were introduced into the SBA-16 cages, and the SBA-16 mesostructure was retained after cobalt impregnation. The Co/SBA-16 catalyst exhibited higher cobalt dispersion compared to the $Co/SiO_2$ catalyst. The catalytic properties of the catalysts in FTS were evaluated in a fixed-bed reactor. The effect of the addition of water was measured in a continuously stirred tank reactor. High FTS activity and stability were observed on the SBA-16-supported catalyst. The SBA-16-supported cobalt catalyst shows low mobility of cobalt particles in the SBA-16 cages. Unlike silica, the SBA-16 support can efficiently prevent the aggregation and sintering of cobalt nanoparticles.

## Introduction

Fischer–Tropsch synthesis (FTS) is a promising process for producing alternative clean fuels from coal, natural gas, and biomass-derived syngas (CO and $H_2$). It aims at converting synthesis gas to long-chain hydrocarbons (FT waxes),[1] and one of the key elements of FTS is the development of active and stable catalysts with high wax selectivity.[2] Cobalt-based catalysts have an advantage over iron-based catalysts because of their high activity, low water gas shift reaction, and higher selectivity to linear paraffin.[3] However, cobalt-based FT catalysts are expensive than iron-based catalysts. Also, a highly active and stable cobalt catalyst is important for ensuring that the process is economically feasible. Under realistic FTS conditions, cobalt-based catalysts exhibited deactivation with time on stream.[4] To maximize the lifetime of a cobalt catalyst, the causes of its deactivation must be eliminated.

In the FTS reaction, the catalyst deactivation is attributed to a combination of phenomena, such as poisoning, sintering, surface carbon formation, carbonization, cobalt reoxidation, cobalt–support interaction compound formation, surface reconstruction, and mechanical deactivation through attrition.[2] The rate and extent of deactivation are also related to process conditions, such as temperature, pressure, conversion, partial pressures of synthesis gas and steam, and the type of reactor (fixed-bed or slurry).

The sintering of a catalyst leads to a reduction of the active surface area, which is thermodynamically driven from the energetically favored surface energy minimization of the crystallites. The two main sintering mechanisms are 1) atomic migration (Ostwald ripening or coarsening) and 2) crystallite migration (coalescence). Sintering processes generally take place at high reaction temperatures and are accelerated by the presence of water vapor.[5] In addition, the size-dependent mobility of the crystals on various supports contributes significantly to sintering. Sintering, in general, is considered to be an irreversible phenomenon. Much attention has been focused on investigating the role of sintering of cobalt in catalyst deactivation. Bartholomew, Bezemer, and co-workers[5] reported that the detrimental effect of water on FT performance was not related to bulk oxidation of cobalt nanoparticles, but rather to water-enhanced sintering. Extended X-ray absorption fine structure results strongly suggested that the deactivation was predominately due to sintering.[6] To obtain a stable catalyst, many preparative methods have been explored, such as embedding active metal within the carbon or silica walls and introducing promoters.[7]

Recently, cubic-structured three-dimensional mesoporous silica (e.g., SBA-16, SBA-1, HOM-9, and KIT-6) have been used as supports for metal, metal oxide, and metal sulfide catalysts.[8] Improved catalyst activities were achieved because these supports reduced agglomeration between particles and hence enhanced the stability of the catalyst and allowed fast transport of reactants and products. The SBA-16 (cubic, *Im*3*m*) with cagelike structures has tunable cage size (4–35 nm) and pore entrance size (generally $<4$ nm).[9] A nanocage is

[a] *Y. Zhao, Y. Zhang*
*College of Chemistry, Chemical Engineering and Materials Science*
*Soochow University*
*Suzhou 215123 (P.R. China)*

[b] *Y. Zhao, Y. Zhang, J. Chen, Prof. J. Li, Prof. K. Liew*
*Key Laboratory of Catalysis and Materials Science*
*of the State Ethnic Affairs Commission & Ministry of Education*
*South-Central University for Nationalities*
*Wuhan 430074 (P.R. China)*
*Fax: (+86) 27-67842752*
*E-mail: jinlinli@yahoo.cn*

[c] *Prof. K. Liew, M. R. B. Nordin*
*Faculty of Industrial Science and Technology*
*University Malaysia Pahang*
*Kuantan 26300 (Malaysia)*

  

interconnected three dimensionally to eight neighboring cages through pore entrances, which are more resistant to blocking and allow smooth transport of reactants and products. The isolated nanocages of SBA-16 can accommodate metal complexes and metal particles formation in situ up to the size of the cage.[8a,b,10] Moreover, the smaller pore entrances may inhibit the migration of metal nanoparticles and hence limit the extent of sintering. Furthermore, SBA-16 has good thermal stability, which is a prerequisite for applications at high temperature, especially in the presence of water.[8c,11]

We report preparation and characterization of SBA-16 cobalt-supported catalysts and their catalytic activity for FTS. The catalysts were characterized by $N_2$ adsorption–desorption, XRD, TEM, and temperature-programmed reduction (TPR). The influence of cobalt loading (10–40 wt% Co) on the FTS performance of Co/SBA-16 catalysts was investigated in a fixed-bed reactor. To better appraise the relative activity and stability of the catalysts, we tested the catalysts for the FTS reaction under the conditions of high CO conversions (in a fixed-bed reactor) and in the presence of high water content in the reaction mixture [in a continuously stirred tank reactor (CSTR)].

## Results and Discussion

### Characterization

#### *$N_2$ adsorption–desorption*

The $N_2$ adsorption–desorption isotherms and pore size distributions of the catalysts are shown in Figure 1. Brunauer–Emmett–Teller (BET) surface areas, pore volumes, and average pore diameters of the catalysts are given in Table 1. The $N_2$ adsorption–desorption isotherms of SBA-16 are type IV ($H_2$) hysteresis loop (see Figure 1a), typical of mesoporous silica with large cages and small opening pores.[12] All the catalysts show two pore size distributions attributed to the pore entrance and the cage and with an average diameter of 3.7 and 10 nm, respectively. The average pore sizes of SBA-16 before and after cobalt loading seem unchanged, which indicates that the pore structure of the SBA-16 support was well preserved after the impregnation of $Co_3O_4$ nanoparticles. As clearly indicated in Table 1, the BET surface areas and pore volumes for the catalysts decreased with increasing cobalt loading, which indicates that cobalt species were introduced into the cages,[13] as also indicated by TEM. BET surface areas, pore volumes, and the pore diameter of 20%Co/$SiO_2$ catalysts are also listed in Table 1, along with those of Co/SBA-16 catalysts.

#### *Transmission electron microscopy*

TEM images of the 20%Co/SBA-16 catalyst (before reduction by $H_2$) are shown in Figure 2a,b. Analysis of Figure 2b reveals that the $Co_3O_4$ nanoparticles are uniformly distributed inside the interconnected cages and most of the $Co_3O_4$ nanoparticles (dark dots) are highly dispersed within the cages along the (111) plane of SBA-16. Shown in Figure 2c is the TEM image of $Co_3O_4$ nanoparticles after removal of $SiO_2$ from the 20%Co/SBA-16 catalysts with use of HF acid. The TEM images indicated that the porous crystals were made of nanoballs connected by nanobridges.[14] Such bridges can be observed at the edge of the particles. The average diameter of the dark dots is 12 nm, which is slightly larger than the cage size of SBA-16. The nonlocal density functional theory (NLDFT) method assumes spherical cages,[15] and therefore calculation of the average particle size from the TEM image is in three dimensions (and possibly include the bridge or the entrance). A careful analysis of many areas of this sample (see Figure 2a) revealed that no larger $Co_3O_4$ particles are located on the external surface of SBA-16 support, which indicates that most of the

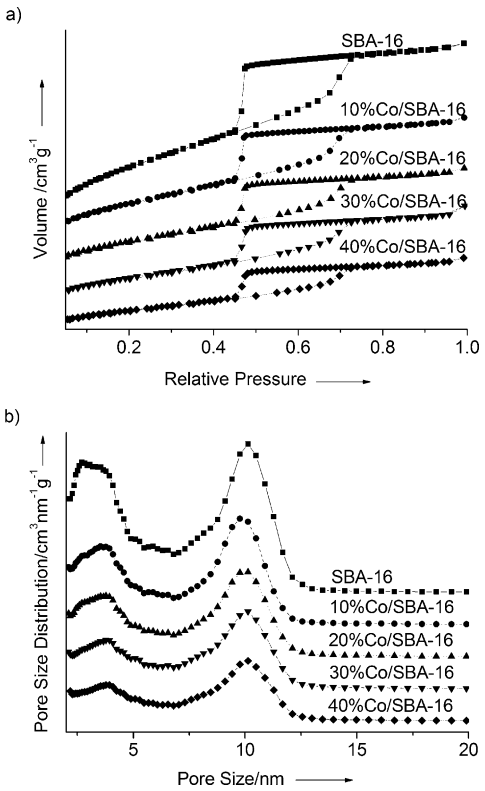


**Figure 1.** a) $N_2$ adsorption–desorption isotherms and b) pore size distributions of the catalysts.

**Table 1.** $N_2$ adsorption–desorption data of catalysts.

| Sample | $V_t$ [$cm^3 g^{-1}$][a] | $S_{BET}$ [$m^2 g^{-1}$][b] | $W_{NLDFT}$ [nm][c] | $D_{Co_3O_4}$ [nm][d] | $D_{Co}$ [nm][e] |
|---|---|---|---|---|---|
| SBA-16 | 0.93 | 1002 | 10.1 (3.5) | | |
| 10%Co/SBA-16 | 0.62 | 640.1 | 10.0 (3.6) | 11.7 | 8.8 |
| 20%Co/SBA-16 | 0.52 | 516.4 | 10.0 (3.7) | 13.2 | 9.9 |
| 30%Co/SBA-16 | 0.48 | 442.4 | 10.1 (3.7) | 11.6 | 8.8 |
| 40%Co/SBA-16 | 0.36 | 330.0 | 10.1 (3.7) | 11.7 | 8.8 |
| $SiO_2$ | 1.24 | 293.2 | 7.0 | | |
| 20%Co/$SiO_2$ | 0.51 | 274.3 | 7.0 | 17.1 | 12.8 |

[a] Total pore volume; [b] BET specific surface area; [c] The pore diameter calculated by means of the NLDFT method from the adsorption branches of the isotherms; [d] Average crystalline size of $Co_3O_4$ calculated from the Scherrer equation; [e] Average cobalt particle size estimated from the corresponding $D_{Co_3O_4}$ by applying the molar volume correction: $D_{Co} = (3/4)D_{Co_3O_4}$.

  

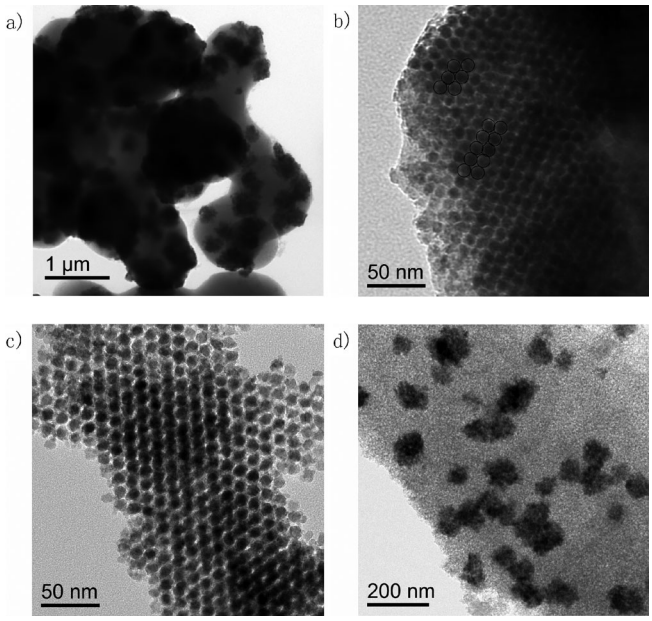


**Figure 2.** TEM images of 20%Co/SBA-16 and 20%Co/$SiO_2$ catalysts before reduction by $H_2$. a) Low magnification image for 20%Co/SBA-16 catalyst. b) (111) projections for 20%Co/S BA-16 catalyst (dark dots are $Co_3O_4$ nanoparticles). c) TEM image of $Co_3O_4$ nanoparticles after removing $SiO_2$ from the 20%Co/SBA-16 catalyst with use of HF acid. d) TEM image of the 20%Co/$SiO_2$ catalyst.

nanoparticles are selectively embedded in the inner pore system of SBA-16. The large cages of the SBA-16 support are only partially filled by $Co_3O_4$, because even if it is fully filled at the beginning by $Co(NO_3)_2{\cdot}6H_2O$, the volume of the cobalt compound will be significantly reduced when it decomposes and forms $Co_3O_4$. Shown in Figure 2d is the TEM image of the referenced 20%Co/$SiO_2$ catalyst (before reduction by $H_2$). Compared with that of the 20%Co/SBA-16, the $Co_3O_4$ particles of this sample are dispersed on the external surface of $SiO_2$ and agglomerate to form islands, which consist of many small $Co_3O_4$ particles. As the contrast between $Co_3O_4$ particles is not sufficiently clear,[16] the $Co_3O_4$ particle size was obtained from the XRD measurement.

Shown in Figure 3 are the TEM images of 20%Co/SBA-16 and 20%Co/$SiO_2$ catalysts after the FTS reaction. It can be observed that the particles inside SBA-16 cages have a remarkable stability against sintering after the reaction (see Figure 3a). This excellent stability is attributed to the unique structure of SBA-16, in which the particles are trapped in the cages and cannot diffuse through the small pore openings connecting the cages. No aggregated particles were observable on the external surface after the reaction because of the three-dimensional structure of the support, although it is expected that the preparation of the catalyst by means of the incipient wetness impregnation method will initially result in a wide range of particle sizes. Shown in Figure 3b is the image of 20%Co/$SiO_2$ catalysts after the reaction. The cobalt particles on used 20%Co/$SiO_2$ catalysts have aggregated into large particles in sizes greater than 17 nm as a result of the sintering process.

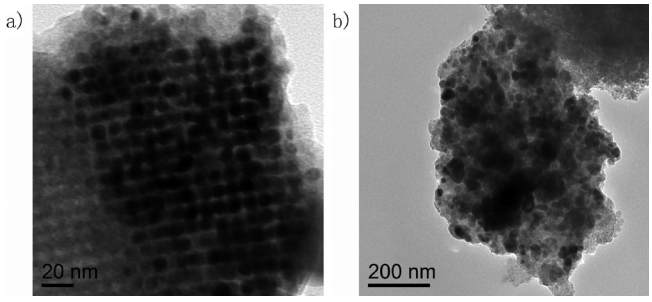


**Figure 3.** TEM images of a) 20%Co/SBA-16 and b) 20%Co/$SiO_2$ catalysts after the reaction. Reaction conditions: 215 °C, 1.0 MPa, $H_2/CO = 2:1$, 3 SL $g^{-1}$ $h^{-1}$ for Co/SBA-16, and 1 SL $g^{-1}$ $h^{-1}$ for Co/$SiO_2$.

### *X-ray diffraction*

Shown in Figure 4 are the low-angle XRD patterns of the Co/SBA-16 catalysts. After impregnation of cobalt, the XRD patterns were almost unchanged and demonstrated the high diffraction peaks at $2\theta = 0.8°$, which reflects the ordered structure of SBA-16. However, with increasing cobalt loading, the intensity of the SBA-16 reflection peak decreased gradually and the peak became broader. The strong reduction of the X-ray peak intensities owes to increasing destructive interferences by the pores filling with increasing amounts of the cobalt oxide, which suggests that cobalt species were highly distributed in the pores.[17]

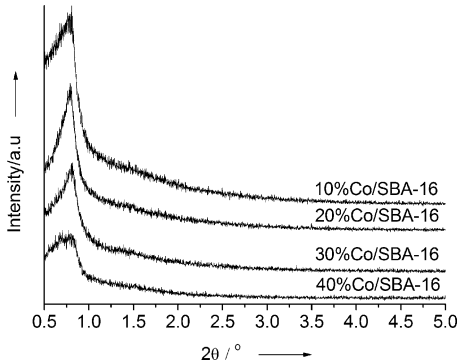


**Figure 4.** Low-angle XRD patterns of the catalysts.

The high-angle XRD patterns for the catalysts are shown in Figure 5. Diffraction peaks at $2\theta = 31.3$, 36.9, 45.1, 59.4, and 65.4° indicate that cobalt is present in the form of $Co_3O_4$ crystalline phase[18] on all the catalysts after calcination at 450 °C. The average particle sizes of $Co_3O_4$ were estimated from the Scherrer equation with use of the most intense reflection at $2\theta = 36.9°$ (see Table 1),[19] which indicates that all the Co/SBA-16 catalysts have similar crystallite size ($\approx$12 nm) which does not increase largely with cobalt loading; this is in good agreement with the TEM results. This also means that most of the cobalt species were impregnated into the cages.

For $SiO_2$ catalysts with the same cobalt loading, the average crystallite size of $Co_3O_4$ calculated from the Scherrer equation

  

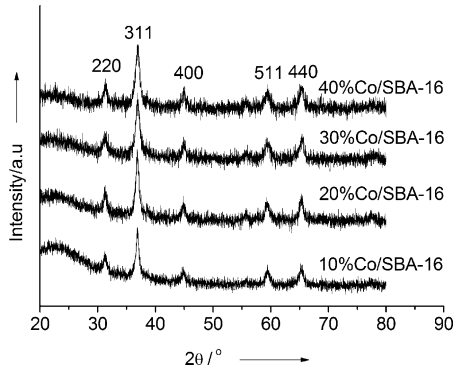


**Figure 5.** High-angle XRD patterns of the catalysts.

is 17.1 nm, larger than that of SBA-16 catalysts and the corresponding pore diameter. This means that most of the $Co_3O_4$ particles were dispersed on the external surface of the $SiO_2$ support, as shown in the TEM images.

### *TPR and $O_2$ titration*

The TPR profiles of the Co/SBA-16 catalysts with different cobalt loadings are shown in Figure 6. For 10%Co/SBA-16 and 20%Co/SBA-16 catalysts, three main reduction peaks are observed. The α peak located at 250–340 °C is attributed to the first step reduction of $Co_3O_4$ ($Co_3O_4 \rightarrow CoO$). The β peak located at 340–390 °C is attributed to the reduction of the intermediate CoO phase ($CoO \rightarrow Co^0$).[20] The relative intensity of the second reduction peak increased with cobalt loading from 10 to 20 wt%, which suggests a higher reduction degree of CoO to Co.[21] A very broad peak (γ peak) located at 550–800 °C and 380–630 °C for 10%Co/SBA-16 and 20%Co/SBA-16 catalysts, respectively, is observed, which indicates the presence of surface cobalt species with different degrees of interaction with the support. As can be seen, the temperature maximum for the γ peak shifted to low temperature with increasing cobalt loading from 10 to 20 wt%, which indicates a lower strength of interaction,[21] attributed to the slightly larger $Co_3O_4$ particle size of 20%Co/SBA-16 catalysts (see Table 1).

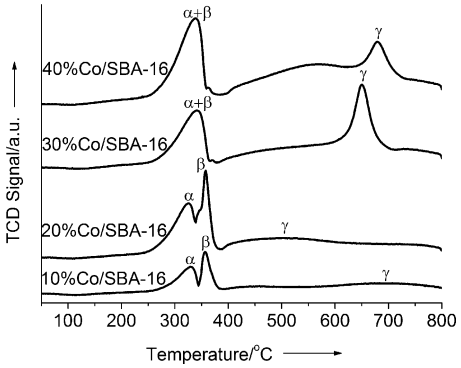


**Figure 6.** TPR profiles of the catalysts.

With increasing cobalt loading, the TPR profiles of 30%Co/SBA-16 and 40%Co/SBA-16 catalysts are significantly different from the other two curves. For 30%Co/SBA-16 and 40%Co/SBA-16 catalysts, two main reduction peaks (α and β) close to each other are observed, with temperature maxima at 250–360 °C. Compared with that of 30%Co/SBA-16 catalyst, the γ peak of 40%Co/SBA-16 became broader and the peak was shifted from 650 to 679 °C. This owes to the fact that with the increase in cobalt loading from 30 to 40 wt%, more cobalt was dispersed on the pore entrance (< 4 nm) of the SBA-16 support. The small $Co_3O_4$ particle in the pore entrance has a stronger interaction with the support. Therefore, the γ peak of the 40%Co/SBA-16 catalyst became broader and the intensity of the peak became stronger. The upshift of the γ peak for 40%Co/SBA-16 implied that the 40%Co/SBA-16 catalyst is more difficult to reduce than is the 30%Co/SBA-16 catalyst.

In summary, the above features indicate that the reducibility of the 20%Co/SBA-16 catalyst is higher than that of 10%Co/SBA-16, 30%Co/SBA-16, and 40%Co/SBA-16 catalysts. The reducibility of the 30%Co/SBA-16 catalyst is higher than that of the 40%Co/SBA-16 catalyst.

The $O_2$ titration data are listed in Table 2, which reveal that the reducibility decreased in the order 20%Co/SBA-16 > 10%Co/SBA-16 > 30%Co/SBA-16 (40%Co/SBA-16). The 30%Co/SBA-16 and 40%Co/SBA-16 catalysts have a similar reducibility. Jacobs et al.[22] reported that for conventional oxide supports, increasing the cobalt loading led to the increased average $Co_3O_4$ particle size and improved reducibility by decreasing the interaction between the metal and the support. However, with the increase in cobalt loading, the $Co_3O_4$ particle size of Co/SBA-16 catalysts could not grow larger than the cage size of SBA-16. Thus, there will be more small particles in the cage entrance with increasing cobalt loading. Increasing cobalt loading from 20 to 30 wt% led to an enhanced interaction between cobalt and SBA-16, and then the reducibility decreased, which are in agreement with the results of TPR.

**Table 2.** $O_2$ titration data of prepared Co/SBA-16 catalysts.

| Sample | $O_2$ uptake [μmol $g^{-1}$] | Reducibility [%] |
|---|---|---|
| 10%Co/SBA-16 | 799.0 | 70.3 |
| 20%Co/SBA-16 | 1659.9 | 73.0 |
| 30%Co/SBA-16 | 2025.6 | 59.4 |
| 40%Co/SBA-16 | 2731.2 | 60.0 |

## Fischer–Tropsch synthesis

### *Effect of cobalt loading*

The catalytic activity of the Co/SBA-16 and $Co/SiO_2$ catalysts was studied in a fixed-bed reactor under typical FTS conditions (210 °C, 1.0 MPa, $H_2/CO = 2:1$, 6 SL $g^{-1}$ $h^{-1}$). The changes in the FTS activity of these catalysts with time on stream are shown in Figure 7. The conversion of CO decreases slightly after 100 h time on stream.

  

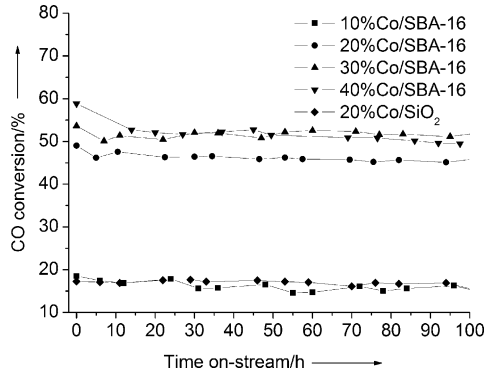


**Figure 7.** FTS activity with time on stream on Co/SBA-16 and $Co/SiO_2$ catalysts. Reaction conditions: 210 °C, 1.0 MPa, 6 SL $g^{-1}$ $h^{-1}$, and $H_2/CO = 2:1$.

The average CO conversion in 100 h on Co/SBA-16 catalysts as a function of cobalt loading is shown in Figure 8. The activity increases with increasing cobalt loading. Increasing cobalt loading from 10 to 20 wt% caused CO conversion to significantly increase from 16 to 46%. A further increase in cobalt loading increased the CO conversion only slightly. The changes in CO conversion as a function of cobalt loading are due to qualitative and quantitative reasons. The quantitative reason is that the increase in cobalt loading provides more cobalt atoms that could potentially serve as the site for the reaction. A further increase in cobalt loading from 30 to 40 wt% seems to achieve a marginal increase in conversion owing to the decrease in the surface area of the catalyst and the lower reducibility owing to the formation of a strong metal–support interaction.

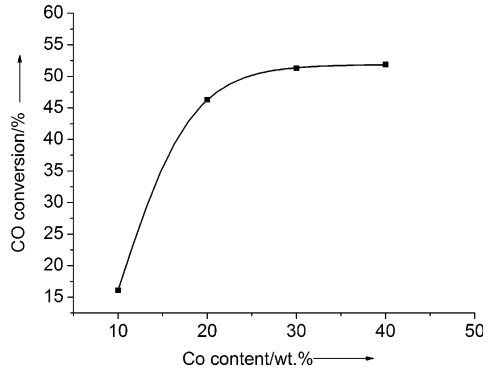


**Figure 8.** Influence of cobalt loading on the CO conversion.

Figure 7 also shows the CO conversion of the 20% $Co/SiO_2$ catalyst (≈16%). The CO conversion of 20% Co/SBA-16 is about three times higher than that of 20% $Co/SiO_2$. This higher activity is related to the higher dispersion of cobalt on the SBA-16 surface because cobalt nanoparticles on SBA-16 have a smaller particle size (see Table 1) and a higher surface area, which makes more cobalt atoms available for FT catalysis.

The data of the FTS activity and product selectivity for the catalysts are summarized in Table 3. Generally, the $C_{5+}$ selectivity increases with increased cobalt particle size. However, in this study, Co/SBA-16 catalysts with a similar particle size have a similar $C_{5+}$ selectivity. However, 10% Co/SBA-16 and 20% Co/$SiO_2$ catalysts, which have different particle sizes and similar CO conversion, have a similar $C_{5+}$ selectivity. This deviation from the generally observed dependence of $C_{5+}$ selectivity on the particle size is attributed to cobalt nanoparticles in the Co/SBA-16 catalyst, which are confined in the cages of the SBA-16 support. The confinement resulted in the repeated readsorption of the α-olefins, which enhanced the chain growth process.[23]

**Table 3.** CO conversion and product distribution of FTS reactions.[a]

| Catalysts | $X_{CO}$ [mol%] | Hydrocarbon selectivity [mol%] | | | | |
|---|---|---|---|---|---|---|
| | | $CH_4$ | $C_2$ | $C_3$ | $C_4$ | $C_{5+}$ |
| 10% Co/SBA-16 | 16.1 | 6.7 | 0.7 | 2.5 | 4.0 | 86.1 |
| 20% Co/SBA-16 | 46.3 | 5.7 | 0.7 | 2.1 | 2.9 | 88.6 |
| 30% Co/SBA-16 | 51.3 | 6.4 | 0.7 | 1.8 | 2.6 | 88.5 |
| 40% Co/SBA-16 | 51.9 | 7.5 | 0.9 | 2.1 | 2.9 | 86.6 |
| 20% $Co/SiO_2$ | 16.5 | 5.2 | 0.7 | 2.3 | 4.7 | 87.1 |

[a] Reaction conditions: 1.0 MPa, 210 °C, $H_2/CO = 2:1$, 6 SL $g^{-1}$ $h^{-1}$; FTS data were collected at steady state (80 h).

### *High CO conversion*

A number of studies have linked FT catalyst deactivation with sintering of cobalt crystallites resulting from high water partial pressures under reaction conditions.[5] When FTS is performed at a high CO conversion (80%), the concentrations of CO and $H_2$ became lower and the concentration of $H_2O$ formed was higher. Under this condition, sintering and hence deactivation will be accelerated. To further explore the advantage of the Co/SBA-16 catalyst, a comparison of the stability of 20% Co/SBA-16 catalyst with that of 20% $Co/SiO_2$ catalysts at a high initial CO conversion (>80%) was studied. This study was conducted by using a fixed-bed reactor at $T = 215$ °C, $P = 1.0$ MPa, and $H_2/CO = 2:1$. The reactant gas flow rate for the 20% Co/SBA-16 catalyst was 3 SL $g^{-1}$ $h^{-1}$ whereas that for the 20% Co/$SiO_2$ catalyst was 1 SL $g^{-1}$ $h^{-1}$. The plots of CO conversion with time on stream are shown in Figure 9. After 100 h time on

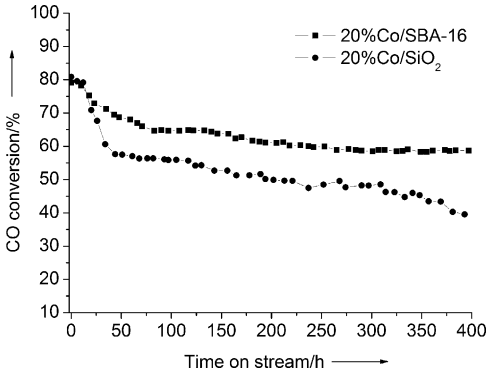


**Figure 9.** FTS activity with time on stream on 20% Co/SBA-16 and 20% Co/$SiO_2$ catalysts. Reaction conditions: 215 °C, 1.0 MPa, $H_2/CO = 2:1$, 3 SL $g^{-1}$ $h^{-1}$ for Co/SBA-16, and 1 SL $g^{-1}$ $h^{-1}$ for $Co/SiO_2$.

  

stream, the CO conversion on the 20%Co/SBA-16 catalyst decreases substantially from 80 to 65%. However, over the next 300 h the CO conversion decreases only by 8%, that is, to 57%. In the case of the $Co/SiO_2$ catalyst, the CO conversion decreases from 80 to 55% in the first 100 h time on stream and then down to 38% after 400 h time on stream. These results confirm that the 20%Co/SBA-16 catalyst is not only much more active but also more stable than the 20%$Co/SiO_2$ catalyst.

Figure 10 shows the CO conversion within 100 h. The loss of activity for the first-step deactivation can be simulated with power-law Expressions (1) and (2):

$$\text{Co/SBA-16 catalyst}: \quad X_{CO} = 95.99\,T_{(h)}^{-0.0865} \tag{1}$$

$$\text{Co/SiO}_2\text{ catalyst}: \quad X_{CO} = 110.88\,T_{(h)}^{-0.1602} \tag{2}$$

in which $X$ is the CO conversion and $T$ is the reaction time.

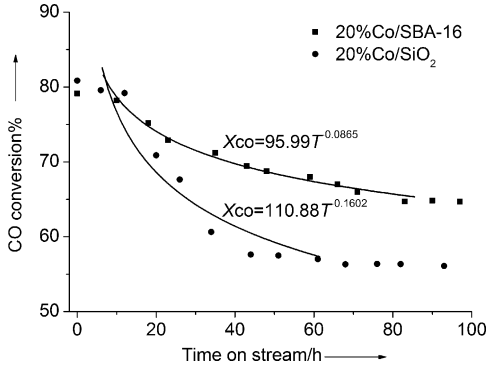


**Figure 10.** FTS activity as a function of time on stream in a run of 100 h on 20%Co/SBA-16 and 20%$Co/SiO_2$ catalysts.

The sintering rate data were fitted to a simple power law expression shown in Equation (3):[5a]

$$-\frac{dX}{dT} = kX^n \tag{3}$$

in which $k$ is the sintering rate constant and $n$ is the sintering order, which may vary from 3 to 15. After integration and data reduction, the sintering order ($n$) is determined to be 12.6 and 7.2 for Co/SBA-16 and $Co/SiO_2$ catalysts, respectively. These values are within the usual range of sintering order, which implies that the activity loss of the first-step deactivation is attributed to the sintering of the small cobalt particles resulting from fewer cobalt particles on the external surface of the support during FTS, in agreement with the observation of Bertole et al.[24] The deactivation in the second step could be due to the collapse of the support, the formation of cobalt silicates, and/or the blockage of microporous channels.[2,25]

As observed in Figures 9 and 10, the 20%Co/SBA-16 catalyst is more active and stable than the 20%$Co/SiO_2$ catalyst, which is attributed to the high dispersion of cobalt species and low mobility of cobalt particles[26] in the SBA-16 cages, respectively. Owing to the spatial restriction of the isolated nanocages and smaller pore entrances of SBA-16, the aggregation and the sintering of cobalt nanoparticles were efficiently prevented. However, for $Co/SiO_2$, the spatial restriction was unable to prevent the growth of cobalt nanoparticles. This is evidenced by TEM analysis (Figure 2d), which confirms that $Co_3O_4$ nanoparticles are located on the external surface of the silica. After the FTS reaction, cobalt nanoparticles were found to have grown up to larger particles (Figure 3b). This result is consistent with previous works.[5b,27]

### *Water effect*

The stability of the Co/SBA-16 catalyst with the addition of water was investigated. The reaction was performed with a CSTR. To keep the partial pressures of $H_2$ and CO constant, 30 vol% of nitrogen was added to the feed at the beginning of the run. Figure 11 shows the changes in CO conversion with time on stream for 20%Co/SBA-16 and 20%$Co/SiO_2$ catalysts.

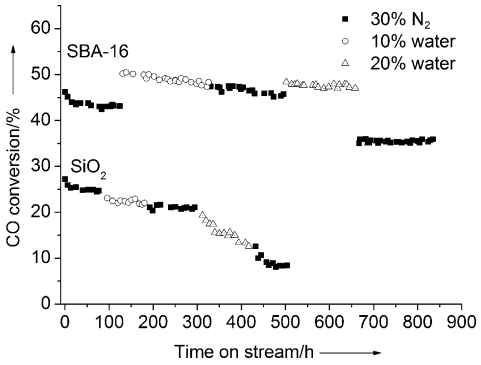


**Figure 11.** FTS activity with time on stream on Co/SBA-16 and $Co/SiO_2$ catalysts with the addition of water. Reaction conditions: 230 °C, 1.0 MPa, 6 SL $h^{-1}$ $g^{-1}$, 30% $N_2$ (standard conditions), $H_2/CO/N_2 = 4.67:2.33:3$, 10% water: $H_2/CO/N_2/H_2O = 4.67:2.33:2:1$, and 20% water: $H_2/CO/N_2/H_2O = 4.67:2.33:1:2$.

For the 20%Co/SBA-16 catalyst, with the feed gases containing 10 vol% of water, the CO conversion was found to be higher than that without water. After switching back to the standard conditions, the CO conversion did not rapidly return to the original activity. However, with the feed gases containing 20 vol% of water, the catalyst still retained the same high activity as that with the feed gas containing 10 vol% of water. During the whole 650 h of reaction, no decrease in CO conversion is observed. After switching back to the standard operating conditions, the CO conversion of the 20%Co/SBA-16 catalyst is lower than the original conversion without water addition and stabilized at 35%.

For the 20%$Co/SiO_2$ catalyst, the 10 vol% of water addition did not affect the rate of catalyst deactivation (0.5% per day). After switching back to the standard conditions, no change in the deactivation rate is observed. However, when 20 vol% of water was added, the CO conversion decreased dramatically and the rate of catalyst deactivation increased significantly (1.4% per day). Even when water addition is stopped, the rate

  

of catalyst deactivation did not change. During the whole 500 h of reaction, the CO conversion decreased from 28 to 8%.

Water appears to have a significant adverse impact on the $Co/SiO_2$ catalyst than on the 20%Co/SBA-16 catalyst. It can be concluded that the CO conversion of 20%Co/SBA-16 increased upon the addition of water whereas the CO conversion of 20%$Co/SiO_2$ decreased rapidly. The high stability of the Co/SBA-16 catalyst is attributed to the effective stabilization of cobalt nanoparticles in the three-dimensional mesoporous silica cages of SBA-16—known as the pore confinement effect. Dalai et al.[28] found that the CO conversion was dramatically increased when water was added to the $Co/SiO_2$ catalyst with particles inside the support pore. Tavasoli et al.[27] reported that the lower sintering rates of the cobalt particles in the inner tube of the carbon nanotubes compared with the particles located on the outer layers were ascribed to a stronger interaction between the cobalt oxides and the inner sides of the carbon nanotubes. Borg et al.[29] showed that an enhanced CO conversion by water addition was due to a diffusion effect in the pores.

## Conclusions

Co/SBA-16 catalysts with different cobalt loadings were prepared by means of the impregnation method. The results of TEM, $N_2$ adsorption–desorption, and XRD analysis showed that most of the $Co_3O_4$ nanoparticles were located inside the SBA-16 cages. High Fischer–Tropsch synthesis (FTS) activity and stability were observed on the 20%Co/SBA-16 catalyst. The CO conversion increased with the cobalt loading up to 20% and then increased slightly with the further increase in cobalt loading. The catalyst deactivation at a high CO conversion and the effect of water addition on the catalyst deactivation were investigated in the fixed-bed reactor and continuously stirred tank reactor, respectively. The results showed that by comparing a commercial $SiO_2$, the high FTS activity and stability of Co/SBA-16 are attributed to the high dispersion of cobalt species and low mobility of cobalt nanoparticles in SBA-16 cages. The isolated nanocages and smaller pore entrances of SBA-16 support efficiently prevented the aggregation and sintering of cobalt nanoparticles, which is one of the main deactivation mechanisms in FTS.

## Experimental Section

SBA-16 was prepared according to published methods by use of poly(ethylene oxide)–poly(propylene oxide)–poly(ethylene oxide) triblock copolymers as templates.[9a–d,11] In a typical preparation of SBA-16, triblock copolymer mixtures [1.2 g of P123 ($EO_{20}PO_{70}EO_{20}$) and 6.0 g of F127 ($EO_{106}PO_{70}EO_{106}$)] were dissolved in HCl (340 mL, 2 M) at RT. Tetraethylorthosilicate (28.28 g) was then added to this mixture, and the mixture was at 35 °C for 24 h. The mixture is then aged at 100 °C for 24 h without stirring. The solid product was filtered, washed with distilled water, and calcined in air at 550 °C for 5 h to remove the template. The $SiO_2$ support used was obtained from Qingdao Meigao Chemical Co.

Co/SBA-16 catalysts with different cobalt loadings (10, 20, 30, and 40 wt%) were prepared by means of incipient wetness impregnation method of the respective SBA-16 with the desired amount of aqueous cobalt nitrate. The wet mass was dried at 120 °C for 12 h, followed by calcination at 450 °C for 5 h. For comparison, $Co/SiO_2$ catalysts with 20 wt% cobalt loading were prepared similarly. The samples were labeled as *x*%Co/SBA-16, in which *x* represents cobalt loading.

A Bruker advanced D8 powder X-ray diffractometer with monochromatic $CuK_\alpha$ radiation and nickel filter equipped with a VANTEC-1 detector was used for XRD measurements. The small and large angle scan ranges were 0.5–5° and 20–80°, respectively, with steps of 0.016°. The average particle sizes of $Co_3O_4$ were estimated from the Scherrer equation with use of the most intense diffraction peak at $2\theta = 36.9°$. TEM analyses of the samples were performed with an FEI TECNAI G2 F20 S-Twin microscope. The samples were crushed in an agate mortar, dispersed in ethanol, and deposited on a copper–carbon grid for observation. $N_2$ adsorption–desorption experiment was conducted at −196 °C with a Quantachrome Autosorb-1-C/TCD/MS. Prior to the experiment, the sample was degassed at 200 °C for 6 h. The surface area was obtained from the adsorption branch by means of the BET model in a relative pressure ranging from 0.05 to 0.30. The total pore volumes were calculated from the amount of $N_2$ vapor adsorbed at a relative pressure of 0.99. The pore size distribution was evaluated from the adsorption branch of the isotherms by means of NLDFT method.[15,30] $H_2$-TPR was performed in a Zeton Altamira AMI-200 unit. Prior to the $H_2$-TPR measurement, the sample (0.05 g) was first flushed with argon (30 $cm^3 min^{-1}$) at 150 °C for 1 h and then cooled down to 50 °C. Ten percent of $H_2$/Ar (30 $cm^3 min^{-1}$) was flown subsequently through the catalyst while the temperature was increased to 800 °C at a rate of 10 °C $min^{-1}$ and held at 800 °C for 30 min. The $H_2$ consumption (thermal conductivity detector signal) was recorded automatically by a PC. The degree of reduction was measured by using oxygen titration conducted in a Zeton Altamira AMI-200 unit. The sample was reduced in pure hydrogen at 450 °C for 12 h and then reoxidized at 450 °C by introducing pulses of high-purity oxygen, which are detected by the thermal conductivity detector located downstream, until there was no further consumption of $O_2$. The reference gas for thermal conductivity detector was high-purity helium. All flow rates were set at 30 $cm^3 min^{-1}$. The extent of catalyst reduction was calculated by assuming stoichiometric reoxidation of Co to $Co_3O_4$. The formula for the calculation has been shown in previous studies.[22]

FTS was performed in a tubular fixed-bed reactor (internal diameter = 12 mm). The Co/SBA-16 sample (0.5 g) was mixed with carborundum (5 g) and then reduced in high-purity $H_2$ (space velocity of 6 NL $h^{-1} g^{-1}$, 25 °C, 101.325 kPa) at atmospheric pressure. The reactor temperature was increased from the ambient temperature to 100 °C (held 60 min) and then increased to 450 °C in 2 h and held for 10 h. The reactor was subsequently cooled down to 150 °C. The syngas ($H_2/CO = 2:1$, space velocity of 6 SL $h^{-1} g^{-1}$, 0 °C, 101.325 kPa) was then switched on, and the pressure was increased to 1.0 MPa. The reaction temperature was increased to 210 °C at 1 °C $min^{-1}$, and the reaction was performed at 210 °C. The products were collected in a hot trap (130 °C) and a cold trap (−2 °C) in sequence. The outlet gases were analyzed online with an Agilent 3000 A GC; the oil collected at −2 °C was analyzed with an Agilent 6890 N GC, whereas the wax collected at 130 °C was analyzed with an Agilent 7890 A GC.

For the high CO conversion test in a fixed-bed reactor, the catalyst (1 g; 20%Co/SBA-16 or 20%$Co/SiO_2$) was mixed with carborun-

  

dum (5 g) and reduced in high-purity $H_2$ (space velocity of 6 NL $h^{-1}$ $g^{-1}$) at 450 °C for 10 h. FTS reactions were performed under the following conditions: $H_2/CO = 2:1$, 1.0 MPa, reaction temperature 215 °C, and space velocity of 3 SL $h^{-1}$ $g^{-1}$ for the 20% Co/SBA-16 catalyst and 1 SL $h^{-1}$ $g^{-1}$ for the 20% Co/$SiO_2$ catalyst.

The effect of water in the reaction mixture on catalytic activities was measured in a CSTR. The appropriate amount of water was injected into the feed gas. The 20% Co/SBA-16 and 20% Co/$SiO_2$ catalysts were used for activity testing. The catalyst activation was conducted first ex situ and then in situ according to the following procedure: The catalyst (10 g) was placed in a fixed-bed reactor and reduced in a flow of high-purity $H_2$ with a space velocity of 6 NL $h^{-1}$ $g^{-1}$ at atmospheric pressure. The reactor temperature was increased from the ambient temperature to 120 °C (held for 60 min) and then increased to 450 °C in 6.5 h (held for 10 h). The reactor was subsequently cooled down to the ambient temperature. The catalyst was transferred under the protection of nitrogen to the CSTR to mix with the melted wax (500 g). The catalyst was then reduced in situ. Hydrogen was introduced to the reactor at atmospheric pressure with a flow rate of 6 NL $h^{-1}$ $g^{-1}$. The reactor temperature was increased to 280 °C at a rate of 120 °C $h^{-1}$ and maintained at this activation condition for 12 h. The FTS reactor system has been described earlier.[31] After the activation, the reactor temperature was decreased to 180 °C and the syngas mixture ($H_2/CO/N_2 = 4.67:2.33:3$, space velocity of 6 SL $h^{-1}$ $g^{-1}$) was introduced to increase the reactor pressure to 1.0 MPa. The reactor temperature was then increased to 230 °C at a rate of 5 °C $h^{-1}$. During the entire run, the reactor temperature was 230 °C and the pressure was 1.0 MPa. The mixed gases entered the CSTR below the stirrer operated at 750 rpm. When water was added, a fraction of nitrogen was replaced by an equal amount of water. Thus, the amount of water added plus nitrogen was 30 vol% of the total feed during the run. The reaction conditions were changed back to the standard conditions after each water addition step. Products were continuously removed from the vapor and passed through two traps, one maintained at 180 °C and the other at −2 °C. The outlet gases were analyzed online with an Agilent 3000 A GC.

## Acknowledgements

*This work was supported by National Natural Science foundation of China (Grant No. 21073238), National Basic Research Program of China (Grant No. 2011CB211704), Natural Science Foundation of Hubei Province of China (Grant No. 2009CDA049), and the Special Fund for Basic Scientific Research of Central Colleges, South-Central University for Nationalities (Grant No. ZZY10005).*

**Keywords:** cobalt · Fischer–Tropsch synthesis · heterogeneous catalysis · mesoporous materials · SBA-16

[1] A. Y. Khodakov, W. Chu, P. Fongarland, *Chem. Rev.* **2007**, *107*, 1692–1744.
[2] N. E. Tsakoumis, M. Rønning, Ø. Borg, E. Rytter, A. Holmen, *Catal. Today* **2010**, *154*, 162–182.
[3] a) E. Iglesia, *Appl. Catal. A* **1997**, *161*, 59–78; b) Q. Zhang, J. Kang, Y. Wang, *ChemCatChem* **2010**, *2*, 1030–1058; c) B. Sun, M. Qiao, K. Fan, J. Ulrich, F. Tao, *ChemCatChem* **2011**, *3*, 542–550.
[4] J. van de Loosdrecht, B. Balzhinimaev, J. A. Dalmon, J. W. Niemantsverdriet, S. V. Tsybulya, A. M. Saib, P. J. van Berge, J. L. Visagie, *Catal. Today* **2007**, *123*, 293–302.
[5] a) C. H. Bartholomew, *Appl. Catal. A* **2001**, *212*, 17–60; b) G. L. Bezemer, T. J. Remans, A. P. van Bavel, A. I. Dugulan, *J. Am. Chem. Soc.* **2010**, *132*, 8540–8541.
[6] G. Jacobs, P. M. Patterson, Y. Zhang, T. Das, J. Li, B. H. Davis, *Appl. Catal. A* **2002**, *233*, 215–226.
[7] a) K. Xiong, J. Li, K. Liew, X. Zhan, *Appl. Catal. A* **2010**, *389*, 173–178; b) J. W. Bae, S. M. Kim, Y. J. Lee, M. J. Lee, K. W. Jun, *Catal. Commun.* **2009**, *10*, 1358–1362; c) A. H. Lu, J. J. Nitz, M. Comotti, C. Weidenthaler, K. Schlichte, C. W. Lehmann, O. Terasaki, F. Schüth, *J. Am. Chem. Soc.* **2010**, *132*, 14152–14162.
[8] a) Z. Ma, H. Yang, Y. Qin, Y. Hao, G. Li, *J. Mol. Catal. A* **2010**, *331*, 78–85; b) L. Li, D. L. King, J. Liu, Q. Huo, K. Zhu, C. Wang, M. Gerber, D. Stevens, Y. Wang, *Chem. Mater.* **2009**, *21*, 5358–5364; c) H. Sun, Q. Tang, Y. Du, X. Liu, Y. Chen, Y. Yang, *J. Colloid Interface Sci.* **2009**, *333*, 317–323.
[9] a) T.-W. Kim, R. Ryoo, M. Kruk, K. P. Gierszal, M. Jaroniec, S. Kamiya, O. Terasaki, *J. Phys. Chem. B* **2004**, *108*, 11480–11489; b) O. C. Gobin, Y. Wan, D. Zhao, F. Kleitz, S. Kaliaguine, *J. Phys. Chem. C* **2007**, *111*, 3053–3058; c) D. Zhao, Q. Huo, J. Feng, B. F. Chmelka, G. D. Stucky, *J. Am. Chem. Soc.* **1998**, *120*, 6024–6036; d) Y. Sakamoto, M. Kaneda, O. Terasaki, D. Y. Zhao, J. M. Kim, G. Stucky, H. J. Shin, R. Ryoo, *Nature* **2000**, *408*, 449–453; e) P. Zhang, Z. Wu, N. Xiao, L. Ren, X. Meng, C. Wang, F. Li, Z. Li, F.-S. Xiao, *Langmuir* **2009**, *25*, 13169–13175.
[10] a) H. Yang, J. Li, J. Yang, Z. Liu, Q. Yang, C. Li, *Chem. Commun.* **2007**, 1086–1088; b) H. Yang, L. Zhang, W. Su, Q. Yang, C. Li, *J. Catal.* **2007**, *248*, 204–212; c) H. Yang, L. Zhang, L. Zhong, Q. Yang, C. Li, *Angew. Chem.* **2007**, *119*, 6985–6989; *Angew. Chem. Int. Ed.* **2007**, *46*, 6861–6865.
[11] M. Kruk, C. M. Hui, *J. Am. Chem. Soc.* **2008**, *130*, 1528–1529.
[12] Y. Kim, X. Guo, G. Kim, *Chem. Commun.* **2009**, 4296–4298.
[13] a) Y. Wang, M. Noguchi, Y. Takahashi, Y. Ohtsuka, *Catal. Today* **2001**, *68*, 3–9; b) H. Yang, G. Zhang, X. Hong, Y. Zhu, *Microporous Mesoporous Mater.* **2004**, *68*, 119–125.
[14] W. Yue, A. H. Hill, A. Harrison, W. Zhou, *Chem. Commun.* **2007**, 2518–2520.
[15] P. I. Ravikovitch, A. V. Neimark, *Langmuir* **2002**, *18*, 1550–1560.
[16] a) S. Storsæter, B. Tøtdal, J. C. Walmsley, B. S. Tanem, A. Holmen, *J. Catal.* **2005**, *236*, 139–152; b) P. Li, J. Liu, N. Nag, P. A. Crozier, *Appl. Catal. A* **2006**, *307*, 212–221; c) M. D. Shannon, C. M. Lok, J. L. Casci, *J. Catal.* **2007**, *249*, 41–51.
[17] M. Fröba, R. Kohn, G. Bouffaud, O. Richard, G. van Tendeloo, *Chem. Mater.* **1999**, *11*, 2858–2865.
[18] a) A. Y. Khodakov, R. Bechara, A. GribovalConstant, *Appl. Catal. A* **2003**, *254*, 273–288; b) E. Lira, C. M. López, F. Oropeza, M. Bartolini, J. Alvarez, M. Goldwasser, F. L. Linares, J. F. Lamonier, M. J. Pérez Zurita, *J. Mol. Catal. A* **2008**, *281*, 146–153.
[19] J. Li, Y. Xu, D. Wu, Y. Sun, *Catal. Today* **2009**, *148*, 148–152.
[20] a) P. Arnoldy, J. A. Moulijn, *J. Catal.* **1985**, *93*, 38–54; b) B. Viswanathan, R. Gopalakrishnan, *J. Catal.* **1986**, *99*, 342–348.
[21] H. Li, S. Wang, F. Ling, J. Li, *J. Mol. Catal. A* **2006**, *244*, 33–40.
[22] G. Jacobs, T. K. Das, Y. Zhang, J. Li, G. Racoillet, B. H. Davis, *Appl. Catal. A* **2002**, *233*, 263–281.
[23] H. Xiong, Y. Zhang, S. Wang, K. Liew, J. Li, *J. Phys. Chem. C* **2008**, *112*, 9706–9709.
[24] C. J. Bertole, C. A. Mims, G. Kiss, *J. Catal.* **2002**, *210*, 84–96.
[25] A. K. Dalai, B. H. Davis, *Appl. Catal. A* **2008**, *348*, 1–15.
[26] Y. Lee, J. Park, K. Jun, J. Bae, P. Sai Prasad, *Catal. Lett.* **2009**, *130*, 198–203.
[27] A. Tavasoli, M. Tre'panier, A. K. Dalai, N. Abatzoglou, *J. Chem. Eng. Data* **2010**, *55*, 2757–2763.
[28] A. K. Dalai, T. K. Das, K. V. Chaudhari, G. Jacobs, B. H. Davis, *Appl. Catal. A* **2005**, *289*, 135–142.
[29] Ø. Borg, S. Storsæter, S. Eri, H. Wigum, E. Rytter, A. Holmen, *Catal. Lett.* **2006**, *107*, 95–102.
[30] M. Jaroniec, L. A. Solovyov, *Langmuir* **2006**, *22*, 6757–6760.
[31] a) J. Li, G. Jacobs, T. Das, Y. Zhang, B. Davis, *Appl. Catal. A* **2002**, *236*, 67–76; b) J. Li, L. Xu, R. Keogh, B. Davis, *Catal. Lett.* **2000**, *70*, 127–130.

Received: July 7, 2011
Revised: September 10, 2011
Published online on December 5, 2011

  